Hybrid Cramér-Rao bound of direction finding, using a triad of cardioid sensors that are perpendicularly oriented and spatially collocated

Dominic Makaa Kitavi
Department of Mathematics, Computing and Information Technology, University of Embu

Kainam Thomas Wong
School of General Engineering, Beihang University

Tsair-Chuan Lin
Department of Statistics, National Taipei University

Yue Ivan Wu[a)]
College of Computer Science, Sichuan University

Cardioid microphones/hydrophones are highly directional acoustical sensors, which enjoy easy availability via numerous commercial vendors for professional use. Collocating three such cardioids in orthogonal orientation to each other, the resulting triad would be sharply directional yet physically compact, while decoupling the incident signal's time-frequency dimensions from its azimuth-elevation directional dimensions, thereby simplifying signal-processing computations. This paper studies such a cardioid triad's azimuth-elevation direction-of-arrival estimation accuracy, which is characterized here by the hybrid Cramér-Rao bound. This analysis allows the cardioidicity index (α) to be stochastically uncertain, applies to any cardioidic order (k), and is valid for any real-valued incident signal regardless of the signal's time-frequency structure.
© 2019 Acoustical Society of America. https://doi.org/10.1121/1.5120521

I. INTRODUCTION

A. The high directionality of a cardioid sensor

The "cardioid" sensor's name stems from its heart-shaped gain response of $[\alpha + (1 - \alpha)\cos(\beta)]\cos^{(k-1)}(\beta)$, where $\beta \in [0, \pi]$ denotes the angle measured with respect to the cardioid sensor's axis, i.e., the straight line joining the $0°$ and the $180°$ on each of the polar plots in Fig. 1. (Please also see Chap. 5 of Ref. 1.) Such a cardioid sensor's heart-shaped gain pattern is largely unidirectional with one dominant front lobe, unlike a "figure-8" sensor's gain pattern with a back lobe equal in height to its front lobe.

The "cardioidicity index," $\alpha \in [0, 1]$, controls the cardioid's directivity.[1] Strictly speaking, the cardioidicity index depends on the wavelength of the incident signal. Hence, should the incident signal's frequency be *in*exactly known or time-varying, the cardioidicity index would likewise be *un*certain.

The order k specifies the power to which the cosine term is raised in the gain response of the cardioid. First-order cardioids date back to at least 1957.[2] Regarding second-order cardioids, please see Ref. 3. On third-order cardioids, please refer to Ref. 4. These higher-order cardioids are often realized by computing the spatial finite differences of data collected by nearby isotropic sensors.[5]

Cardioid microphones/hydrophones are among the most practical acoustical sensors in wide professional use. For introductions, please see the following books: Chaps. 5, 6, and 11–21 of Ref. 1; Chaps. 8.3–8.5 of Ref. 2; Chaps. 2.5 and 3.4 of Ref. 6; Chaps. 4.5.6 and 4.5.7 of Ref. 7; Chaps. 3.5–3.7, 5.1–5.5, and 5.8 of Ref. 8; and pp. 111–114, 134–135, 342, and 484 of Ref. 9.

Dating back to at least the 1930s,[2,10,11] cardioid microphones are also commercially available from various companies, including

(i)   Models 414, C519M, and SE300B, from AKG Acoustics Company (Vienna, Austria);
(ii)   Models 42, 2020, 4033, 4050, from Audio-Technica Corporation (Tokyo, Japan);
(iii) Model B-2 PRO from Behringer Company (Willich, North Rhine-Westphalia, Germany);
(iv)   Model GXL1200BP from CAD Audio Company (Solon, OH, USA);
(v)   Model Stealthy Cardioid from Core Sound LLC (Teaneck, NJ, USA);
(vi)   d:screet mini 4080 from DPA Microphones Company (Alleroed, Denmark);
(vii) Model MXL 770 from Marshall Electronics Inc. (Torrance, CA, USA);
(viii) Model NT4 from Røde Microphones LLC (Silverwater, New South Wales, Australia);
(ix)   Models Evolution 914 and 935 from Sennheiser Company (Wedemark, Lower Saxony, Germany);
(x)   Models BETA 98A and SM58 from Shure Inc., (Niles, IL, USA); and
(xi)   Model MKV Microphone from SoundField Ltd. (Silverwater, New South Wales, Australia).
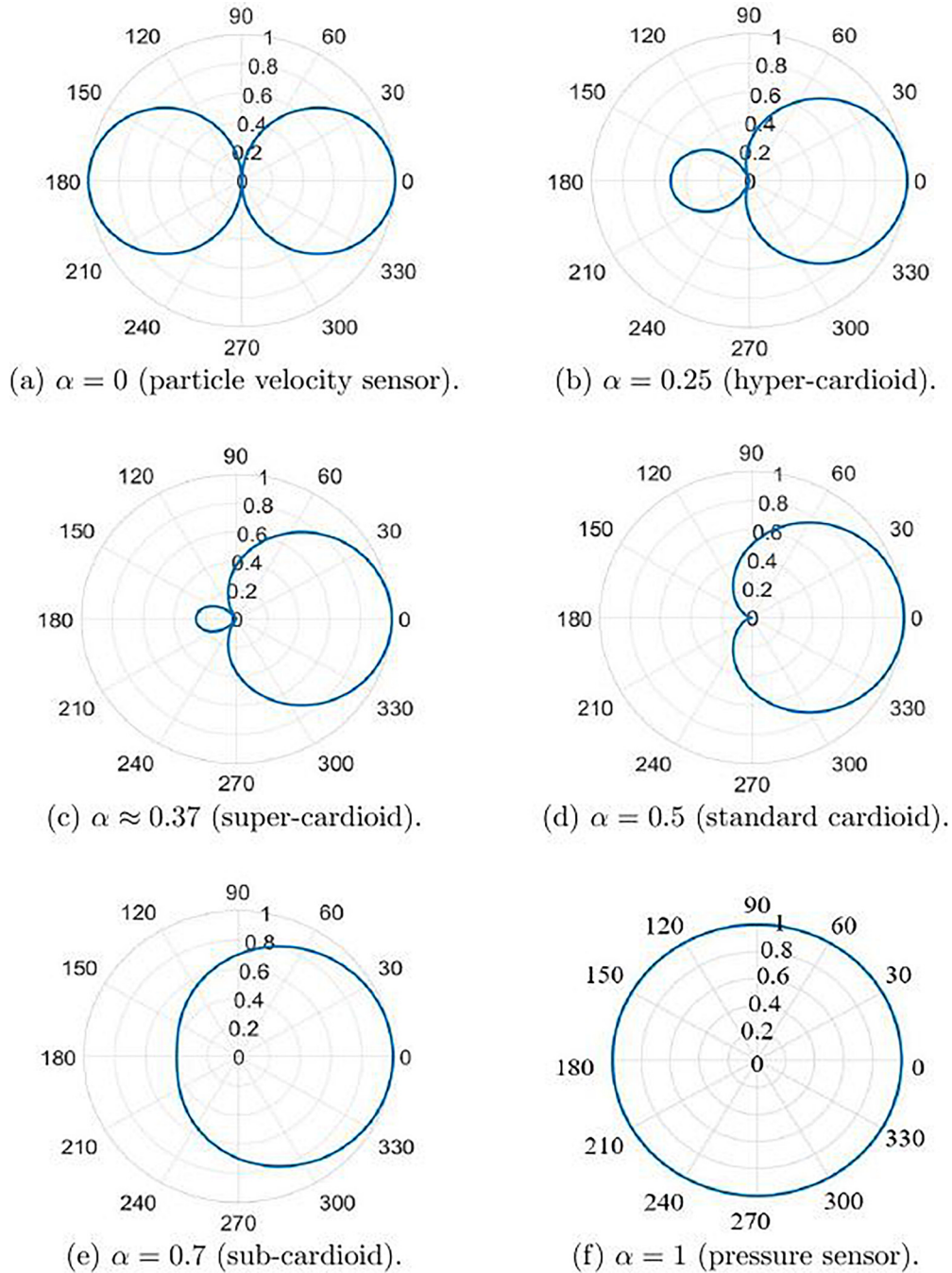
a)Electronic mail: y.i.wu@ieee.org

(a) $\alpha = 0$ (particle velocity sensor).

(b) $\alpha = 0.25$ (hyper-cardioid).

(c) $\alpha \approx 0.37$ (super-cardioid).

(d) $\alpha = 0.5$ (standard cardioid).

(e) $\alpha = 0.7$ (sub-cardioid).

(f) $\alpha = 1$ (pressure sensor).

FIG. 1. (Color online) The cardioid's directivity pattern at order $k = 1$ and various cardioidicity α.

B. The advantages of placing cardioid sensors in orthogonal orientation and in spatial collocation

Consider three kth-order cardioid sensors all collocating at the Cartesian origin, but oriented along the x, y, and z axes. Please see Fig. 2. Such a collocated triad's physical compactness provides the advantage of deployment versatility and easy mobility.

Upon this triad, consider a unit-power signal incident from a polar angle of $\theta \in [0, \pi]$ measured from the positive z axis, and an azimuth angle of $\phi \in [0, 2\pi)$ measured from the positive x axis. The triad's response may be characterized by a 3×1 array manifold[12] of

$$
\mathbf{a}^{(k)} := \begin{bmatrix} [\alpha + (1 - \alpha) \sin(\theta) \cos(\phi)] \sin^{k-1}(\theta) \cos^{k-1}(\phi) \\ [\alpha + (1 - \alpha) \sin(\theta) \sin(\phi)] \sin^{k-1}(\theta) \sin^{k-1}(\phi) \\ [\alpha + (1 - \alpha) \cos(\theta)] \cos^{k-1}(\theta) \end{bmatrix}.
$$

(1)

At $k = 1$ and $\alpha = 0$, the cardioid triad degenerates to the much studied tri-axial velocity-sensor.[13–18]

The above array manifold is *in*dependent of frequency. That is, the spatial collocation uncouples the incident signal's time-frequency dimensions from the azimuth-elevation directional dimensions. This decoupling is most consequential for signal-processing computations. Consider this sample
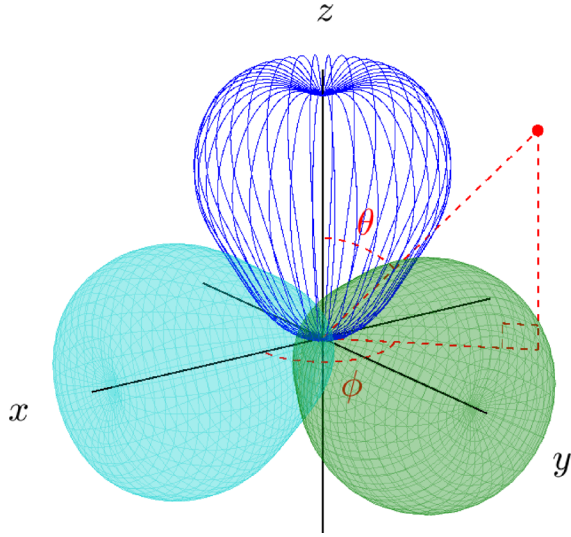
FIG. 2. (Color online) A triad of directional sensors, orthogonally oriented and collocated as one compact unit at the spherical coordinates' origin.

grid of $\mathcal{S}_{T,F} \times \mathcal{S}_{az} \times \mathcal{S}_{el}$, where $\mathcal{S}_{T,F}, \mathcal{S}_{az}, \mathcal{S}_{el}$ refer to the grid size along the time-frequency dimensions, in azimuth, in elevation, respectively. If the three coupled domains become *un*coupled, the product reduces by orders-of-magnitude to only a sum of $\mathcal{S}_{T,F} + \mathcal{S}_{az} \times \mathcal{S}_{el}$.

This idea (of *collocating* diversely oriented cardioids of arbitrary order and arbitrary cardioidicity index) seems to be new to the open literature on direction finding to the present authors' best knowledge. A triad of collocating/perpendicular *first*-order cardioids has been studied in Refs. 12 and 19 for data-*in*dependent beamforming but not for direction finding. This three-dimensionally orthogonal triad differs from the two-dimensional triplet of Refs. 20 and 21 where three first-order standard cardioids (i.e., $k = 1$ and $\alpha = 0.5$) all lie on a flat plane, 120° apart of each other in orientation. Reference 22 collocates four first-order standard cardioids all on a flat plane, 90° apart of each other in orientation. Reference 22 also collocates six first-order standard cardioids with two pointing along the $\pm x$ axes, two along the $\pm y$ axes, and two along the $\pm z$ axes.

To ease subsequent discussion, re-express Eq. (1) in terms of the Cartesian direction cosines $u := \sin(\theta)\cos(\phi)$, $v := \sin(\theta)\sin(\phi)$, $w := \cos(\theta)$, as

$$\mathbf{a}^{(k)} = \begin{bmatrix} [\alpha + (1-\alpha)u]u^{k-1} \\ [\alpha + (1-\alpha)v]v^{k-1} \\ [\alpha + (1-\alpha)w]w^{k-1} \end{bmatrix}. \quad (2)$$

Note that $u^2 + v^2 + w^2 = 1, \ \forall \theta, \forall \phi$.

II. THE DATA MODEL

A cardioid may be effectively formed from a uniaxial velocity-sensor and a pressure-sensor (or from three pressure-sensors) by computing the finite difference among their data. Please see Refs. 23–32 for details. However, the above implementation can be imprecise in the real world. All practical sensors are imperfect.

Hence, the cardioids' α is modeled here as stochastic and normally distributed with a mean of $\bar{\alpha}$ and a standard deviation

of $\sigma_\alpha \ll 1$. This $\sigma_\alpha \ll 1$ presumption helps to render the probability of $\alpha \notin [0, 1]$ to be negligible; this presumption would be reasonable for any well-built sensor for practical use. Deterministically unknown but to be estimated are θ and ϕ.

To avert extraneous distraction from the present work's focus on the uncertainty in α in the cardioids, a simple statistical model is used below. More complex scenarios can be handled in analogy to the analysis below.

Incident upon a cardioid triad is a real-valued signal $\{s(m), \forall m\}$ of *any* time-frequency signal structure. Here, m denotes the discrete-time index. At the mth time-instant, the following 3×1 data are measured by the triad:

$$\mathbf{z}(m) = \mathbf{a}^{(k)}s(m) + \mathbf{n}(m), \quad m = 1, \ldots, M. \quad (3)$$

Here, $\mathbf{n}(m)$ denotes the additive noise's 3×1 vector, whose elements are each modeled as real-valued Gaussian, with a mean of zero and a variance of σ_n^2. This $\mathbf{n}(m)$ is modeled also as statistically uncorrelated over time (i.e., over m) and across the three cardioids, hence, $\mathbf{n}(k) \sim \mathcal{N}(\mathbf{0}_3, \sigma_n^2\mathbf{I}_3)$. In the above, $\mathbf{0}_J$ denotes a $J \times 1$ zero vector, whereas $\mathbf{I}_J$ represents a $J \times J$ identity matrix.

All M number of discrete-time samples may be collected into a $3M \times 1$ vector of

$$\mathbf{z} := \left[\{\mathbf{z}(1)\}^T, \{\mathbf{z}(2)\}^T, \ldots, \{\mathbf{z}(M)\}^T\right]^T$$
$$= \mathbf{s} \otimes \mathbf{a}^{(k)} + \mathbf{n}. \quad (4)$$

The conditional data vector $\mathbf{z}|\alpha$ has a mean of

$$\boldsymbol{\mu} = E\left[\{\mathbf{s} \otimes \mathbf{a}^{(k)} + \mathbf{n}\}|\alpha\right]$$
$$= E\left[\{\mathbf{s} \otimes \mathbf{a}^{(k)}\}|\alpha\right] + E[\mathbf{n}|\alpha]$$
$$= \mathbf{s} \otimes \mathbf{a}^{(k)}, \quad (5)$$

and a covariance matrix of

$$\Gamma = E\left[(\mathbf{z} - \boldsymbol{\mu})(\mathbf{z} - \boldsymbol{\mu})^T|\alpha\right]$$
$$= E[\mathbf{n}\mathbf{n}^T]$$
$$= \sigma_n^2\mathbf{I}_{3M}, \quad (6)$$

where

$$\mathbf{n} := \left[\{\mathbf{n}(1)\}^T, \{\mathbf{n}(2)\}^T, \ldots, \{\mathbf{n}(M)\}^T\right]^T,$$
$$\mathbf{s} := [s(1), s(2), \ldots, s(M)]^T.$$

III. HYBRID CRAMÉR-RAO BOUND DERIVATION FOR CARDIOIDS OF ANY ORDER K

Collect all three unknown scalar parameters into a vector $\boldsymbol{\xi} := [\theta, \phi, \alpha]^T$. From Eqs. (8.49), (8.59), and (8.60) of Ref. 33, the "hybrid Fisher information matrix" (HFIM) equals

$$\mathbf{F}(\boldsymbol{\xi}) := \begin{bmatrix} F_{\theta,\theta} & F_{\theta,\phi} & F_{\theta,\alpha} \\ F_{\theta,\phi} & F_{\phi,\phi} & F_{\phi,\alpha} \\ F_{\theta,\alpha} & F_{\phi,\alpha} & F_{\alpha,\alpha} \end{bmatrix}$$
$$= E_\alpha[\mathbf{H}(\boldsymbol{\xi})] + \begin{bmatrix} \mathbf{0}_{2\times2} & \mathbf{0}_{2\times1} \\ \mathbf{0}_{1\times2} & \sigma_\alpha^{-2} \end{bmatrix}, \quad (7)$$

where $\mathbf{0}_{i,j}$ refers to an $\mathbf{I} \times \mathbf{J}$ matrix of all zero entries.

The (i,j)th element of $\mathbf{H}(\boldsymbol{\xi})$ is given by

$$[\mathbf{H}(\boldsymbol{\xi})]_{i,j} := \left[\frac{\partial \boldsymbol{\mu}}{\partial [\xi]_i}\right]^T \boldsymbol{\Gamma}^{-1} \frac{\partial \boldsymbol{\mu}}{\partial [\xi]_j} + \frac{1}{2}\mathrm{Tr}\left\{\boldsymbol{\Gamma}^{-1}\frac{\partial \boldsymbol{\Gamma}}{\partial [\xi]_i}\boldsymbol{\Gamma}^{-1}\frac{\partial \boldsymbol{\Gamma}}{\partial [\xi]_j}\right\} = \frac{1}{\sigma_n^2}\left[\frac{\partial \boldsymbol{\mu}}{\partial [\xi]_i}\right]^T \frac{\partial \boldsymbol{\mu}}{\partial [\xi]_j} = \frac{1}{\sigma_n^2}\left[\mathbf{s}\otimes\frac{\partial \mathbf{a}^{(k)}}{\partial [\xi]_i}\right]^T\left[\mathbf{s}\otimes\frac{\partial \mathbf{a}^{(k)}}{\partial [\xi]_j}\right]$$

$$= \frac{\mathbf{s}^T\mathbf{s}}{\sigma_n^2}\left[\frac{\partial \mathbf{a}^{(k)}}{\partial [\xi]_i}\right]^T \frac{\partial \mathbf{a}^{(k)}}{\partial [\xi]_j}, \tag{8}$$

where $\mathrm{Tr}\{\cdot\}$ denotes the trace of the matrix inside the curly brackets, and

$$\frac{\partial \mathbf{a}^{(k)}}{\partial \theta} = \begin{bmatrix} \{\alpha(k-1)+k(1-\alpha)\sin(\theta)\cos(\phi)\}\cos(\theta)\sin^{k-2}(\theta)\cos^{k-1}(\phi) \\ \{\alpha(k-1)+k(1-\alpha)\sin(\theta)\sin(\phi)\}\cos(\theta)\sin^{k-2}(\theta)\sin^{k-1}(\phi) \\ -\{\alpha(k-1)+k(1-\alpha)\cos(\theta)\}\sin(\theta)\cos^{k-2}(\theta) \end{bmatrix}, \tag{9}$$

$$\frac{\partial \mathbf{a}^{(k)}}{\partial \phi} = \begin{bmatrix} -\{\alpha(k-1)+k(1-\alpha)\sin(\theta)\cos(\phi)\}\sin(\phi)\cos^{k-2}(\phi)\sin^{k-1}(\theta) \\ \{\alpha(k-1)+k(1-\alpha)\sin(\theta)\sin(\phi)\}\cos(\phi)\sin^{k-2}(\phi)\sin^{k-1}(\theta) \\ 0 \end{bmatrix}, \tag{10}$$

$$\frac{\partial \mathbf{a}^{(k)}}{\partial \alpha} = \begin{bmatrix} \{1-\sin(\theta)\cos(\phi)\}\sin^{k-1}(\theta)\cos^{k-1}(\phi) \\ \{1-\sin(\theta)\sin(\phi)\}\sin^{k-1}(\theta)\sin^{k-1}(\phi) \\ \{1-\cos(\theta)\}\cos^{k-1}(\theta) \end{bmatrix}. \tag{11}$$

Substitute Eqs. (9)–(11) in Eq. (8)

$$H_{\theta,\theta} = \frac{\mathbf{s}^T\mathbf{s}}{\sigma_n^2}\left[\frac{\partial \mathbf{a}^{(k)}}{\partial \theta}\right]^T \frac{\partial \mathbf{a}^{(k)}}{\partial \theta} = \frac{\mathbf{s}^T\mathbf{s}}{\sigma_n^2}\frac{4}{\sin^2(2\theta)}\Bigg[k^2(1-\alpha)^2\{\sin^4(\theta)\cos^{2k}(\theta)+\cos^4(\theta)\sin^{2k}(\theta)[\sin^{2k}(\phi)+\cos^{2k}(\phi)]\}$$

$$+\frac{4\alpha^2(k-1)^2}{\sin^2(2\phi)\sin^2(2\theta)}\{\sin^2(2\phi)\sin^6(\theta)\cos^{2k}(\theta)+4\cos^6(\theta)\sin^{2k}(\theta)[\cos^2(\phi)\sin^{2k}(\phi)+\sin^2(\phi)\cos^{2k}(\phi)]\}$$

$$+\frac{4\alpha k(k-1)(1-\alpha)}{\sin(2\phi)\sin(2\theta)}\{\sin(2\phi)\sin^5(\theta)\cos^{2k}(\theta)+2\cos^5(\theta)\sin^{2k}(\theta)[\cos(\phi)\sin^{2k}(\phi)+\sin(\phi)\cos^{2k}(\phi)]\}\Bigg], \tag{12}$$

$$H_{\theta,\phi} = H_{\phi,\theta} = \frac{\mathbf{s}^T\mathbf{s}}{\sigma_n^2}\left[\frac{\partial \mathbf{a}^{(k)}}{\partial \theta}\right]^T \frac{\partial \mathbf{a}^{(k)}}{\partial \phi} = 2\frac{\mathbf{s}^T\mathbf{s}}{\sigma_n^2}\frac{\cos(\theta)\sin^{2k-1}(\theta)}{\sin(2\phi)}\Bigg[k^2\{1-\alpha\}^2\{\cos^2(\phi)\sin^{2k}(\phi)-\sin^2(\phi)\cos^{2k}(\phi)\}$$

$$+\frac{4\alpha k\{k-1\}\{1-\alpha\}}{\sin(2\phi)\sin(\theta)}\{\cos^3(\phi)\sin^{2k}(\phi)-\sin^3(\phi)\cos^{2k}(\phi)\}$$

$$+\frac{4\alpha^2(k-1)^2}{\sin^2(2\phi)\sin^2(\theta)}\{\cos^4(\phi)\sin^{2k}(\phi)-\sin^4(\phi)\cos^{2k}(\phi)\}\Bigg], \tag{13}$$

$$H_{\theta,\alpha} = H_{\alpha,\theta} = \frac{\mathbf{s}^T\mathbf{s}}{\sigma_n^2}\left[\frac{\partial \mathbf{a}^{(k)}}{\partial \theta}\right]^T \frac{\partial \mathbf{a}^{(k)}}{\partial \alpha} = \frac{\mathbf{s}^T\mathbf{s}}{\sigma_n^2}\frac{4}{\sin(2\phi)\sin^2(2\theta)}\Big[k(1-\alpha)\{[\cos(\theta)-1]\sin(2\phi)\sin^3(\theta)\cos^{2k}(\theta)$$

$$+\cos^3(\theta)\sin^{2k}(\theta)[2\cos(\phi)\sin^{2k}(\phi)+2\sin(\phi)\cos^{2k}(\phi)-\sin(2\phi)\sin(\theta)\{\sin^{2k}(\phi)+\cos^{2k}(\phi)\}]\}$$

$$+\frac{2\alpha(k-1)}{\sin(2\phi)\sin(2\theta)}\{[\cos(\theta)-1]\sin^2(2\phi)\sin^4(\theta)\cos^{2k}(\theta)+2\cos^4(\theta)\sin^{2k}(\theta)$$

$$\times[2\cos^2(\phi)\sin^{2k}(\phi)+2\sin^2(\phi)\cos^{2k}(\phi)-\sin(2\phi)\sin(\theta)\{\cos(\phi)\sin^{2k}(\phi)+\sin(\phi)\cos^{2k}(\phi)\}]\}\Big], \tag{14}$$

$$H_{\phi,\phi} = \frac{\mathbf{s}^T\mathbf{s}}{\sigma_n^2}\left[\frac{\partial \mathbf{a}^{(k)}}{\partial \phi}\right]^T \frac{\partial \mathbf{a}^{(k)}}{\partial \phi} = \frac{\mathbf{s}^T\mathbf{s}}{\sigma_n^2}\frac{4\sin^{2k}(\theta)}{\sin^2(2\phi)}\Big[k^2(1-\alpha)^2\{\cos^4(\phi)\sin^{2k}(\phi)+\sin^4(\phi)\cos^{2k}(\phi)\}$$

$$+\frac{4\alpha^2(k-1)^2}{\sin^2(2\phi)\sin^2(\theta)}\{\cos^6(\phi)\sin^{2k}(\phi)+\sin^6(\phi)\cos^{2k}(\phi)\}$$

$$+\frac{4\alpha k(k-1)(1-\alpha)}{\sin(2\phi)\sin(\theta)}\{\cos^5(\phi)\sin^{2k}(\phi)+\sin^5(\phi)\cos^{2k}(\phi)\}\Big], \tag{15}$$

$$H_{\phi,\alpha} = H_{\alpha,\phi} = \frac{\mathbf{s}^T \mathbf{s}}{\sigma_n^2} \left[\frac{\partial \mathbf{a}^{(k)}}{\partial \phi}\right]^T \frac{\partial \mathbf{a}^{(k)}}{\partial \alpha} = 4 \frac{\mathbf{s}^T \mathbf{s}}{\sigma_n^2} \frac{\sin^{2k-1}(\theta)}{\sin^2(2\phi)} \left[k(1-\alpha)\{[1 - \sin(\phi)\sin(\theta)]\cos^3(\phi)\sin^{2k}(\phi)\right.$$

$$+ [\cos(\phi)\sin(\theta) - 1]\sin^3(\phi)\cos^{2k}(\phi)\} + \frac{2\alpha(k-1)}{\sin(2\phi)\sin(\theta)}\{[1 - \sin(\phi)\sin(\theta)]\cos^4(\phi)\sin^{2k}(\phi)$$

$$\left. + [\cos(\phi)\sin(\theta) - 1]\sin^4(\phi)\cos^{2k}(\phi)\}\right], \tag{16}$$

$$H_{\alpha,\alpha} = \frac{\mathbf{s}^T \mathbf{s}}{\sigma_n^2} \left[\frac{\partial \mathbf{a}^{(k)}}{\partial \alpha}\right]^T \frac{\partial \mathbf{a}^{(k)}}{\partial \alpha} = \frac{\mathbf{s}^T \mathbf{s}}{\sigma_n^2} \left[4 \frac{\sin^{2k-2}(\theta)}{\sin^2(2\phi)}\{[\sin(\phi)\sin(\theta) - 1]^2 \cos^2(\phi)\sin^{2k}(\phi)\right.$$

$$\left. + [\cos(\phi)\sin(\theta) - 1]^2 \sin^2(\phi)\cos^{2k}(\phi)\} + \{\cos(\theta) - 1\}^2 \cos^{2k-2}(\theta)\right]. \tag{17}$$

Substitute Eqs. (12)–(17) in Eq. (7)

$$F_{\theta,\theta} = E_\alpha[H_{\theta,\theta}] = \frac{\mathbf{s}^T \mathbf{s}}{\sigma_n^2} \frac{4}{\sin^2(2\theta)} \left[k^2\{(1-\bar{\alpha})^2 + \sigma_\alpha^2\}\{\sin^4(\theta)\cos^{2k}(\theta) + \cos^4(\theta)\sin^{2k}(\theta)[\sin^{2k}(\phi) + \cos^{2k}(\phi)]\}\right.$$

$$+ \frac{4(k-1)^2(\bar{\alpha}^2 + \sigma_\alpha^2)}{\sin^2(2\phi)\sin^2(2\theta)}\{\sin^2(2\phi)\sin^6(\theta)\cos^{2k}(\theta) + 4\cos^6(\theta)\sin^{2k}(\theta)[\cos^2(\phi)\sin^{2k}(\phi) + \sin^2(\phi)\cos^{2k}(\phi)]\}$$

$$\left. + \frac{4k(k-1)[\bar{\alpha}(1-\bar{\alpha}) - \sigma_\alpha^2]}{\sin(2\phi)\sin(2\theta)}\{\sin(2\phi)\sin^5(\theta)\cos^{2k}(\theta) + 2\cos^5(\theta)\sin^{2k}(\theta)[\cos(\phi)\sin^{2k}(\phi) + \sin(\phi)\cos^{2k}(\phi)]\}\right], \tag{18}$$

$$F_{\theta,\phi} = F_{\phi,\theta} = E_\alpha[H_{\theta,\phi}] = 2\frac{\mathbf{s}^T \mathbf{s}}{\sigma_n^2} \frac{\cos(\theta)\sin^{2k-1}(\theta)}{\sin(2\phi)} \left[k^2\{(1-\bar{\alpha})^2 + \sigma_\alpha^2\}\{\cos^2(\phi)\sin^{2k}(\phi) - \sin^2(\phi)\cos^{2k}(\phi)\}\right.$$

$$+ \frac{4\{k-1\}^2\{\bar{\alpha}^2 + \sigma_\alpha^2\}}{\sin^2(2\phi)\sin^2(\theta)}\{\cos^4(\phi)\sin^{2k}(\phi) - \sin^4(\phi)\cos^{2k}(\phi)\}$$

$$\left. + \frac{4k(k-1)[\bar{\alpha}(1-\bar{\alpha}) - \sigma_\alpha^2]}{\sin(2\phi)\sin(\theta)}\{\cos^3(\phi)\sin^{2k}(\phi) - \sin^3(\phi)\cos^{2k}(\phi)\}\right], \tag{19}$$

$$F_{\theta,\alpha} = F_{\alpha,\theta} = E_\alpha[H_{\theta,\alpha}] = \frac{\mathbf{s}^T \mathbf{s}}{\sigma_n^2} \frac{4}{\sin(2\phi)\sin^2(2\theta)} \left[k(1-\bar{\alpha})\{[\cos(\theta) - 1]\sin(2\phi)\sin^3(\theta)\cos^{2k}(\theta)\right.$$

$$+ \cos^3(\theta)\sin^{2k}(\theta)[2\cos(\phi)\sin^{2k}(\phi) + 2\sin(\phi)\cos^{2k}(\phi) - \sin(2\phi)\sin(\theta)\{\sin^{2k}(\phi) + \cos^{2k}(\phi)\}]\}$$

$$+ \frac{2\bar{\alpha}(k-1)}{\sin(2\phi)\sin(2\theta)}\{[\cos(\theta) - 1]\sin^2(2\phi)\sin^4(\theta)\cos^{2k}(\theta) + 2\cos^4(\theta)\sin^{2k}(\theta)$$

$$\left. \times [2\cos^2(\phi)\sin^{2k}(\phi) + 2\sin^2(\phi)\cos^{2k}(\phi) - \sin(2\phi)\sin(\theta)\{\cos(\phi)\sin^{2k}(\phi) + \sin(\phi)\cos^{2k}(\phi)\}]\}\right], \tag{20}$$

$$F_{\phi,\phi} = E_\alpha[H_{\phi,\phi}] = 4\frac{\mathbf{s}^T \mathbf{s}}{\sigma_n^2} \frac{\sin^{2k}(\theta)}{\sin^2(2\phi)} \left[k^2\{(1-\bar{\alpha})^2 + \sigma_\alpha^2\}\{\cos^4(\phi)\sin^{2k}(\phi) + \sin^4(\phi)\cos^{2k}(\phi)\}\right.$$

$$+ \frac{4(k-1)^2\{\bar{\alpha}^2 + \sigma_\alpha^2\}}{\sin^2(2\phi)\sin^2(\theta)}\{\cos^6(\phi)\sin^{2k}(\phi) + \sin^6(\phi)\cos^{2k}(\phi)\}$$

$$\left. + \frac{4k(k-1)\{\bar{\alpha}(1-\bar{\alpha}) - \sigma_\alpha^2\}}{\sin(2\phi)\sin(\theta)}\{\cos^5(\phi)\sin^{2k}(\phi) + \sin^5(\phi)\cos^{2k}(\phi)\}\right], \tag{21}$$

$$F_{\phi,\alpha} = F_{\alpha,\phi} = E_\alpha[H_{\phi,\alpha}] = 4\frac{\mathbf{s}^T \mathbf{s}}{\sigma_n^2} \frac{\sin^{2k-1}(\theta)}{\sin^2(2\phi)} \left[k\{1-\bar{\alpha}\}\{[1 - \sin(\phi)\sin(\theta)]\cos^3(\phi)\sin^{2k}(\phi) + [\cos(\phi)\sin(\theta) - 1]\right.$$

$$\left. \times \sin^3(\phi)\cos^{2k}(\phi)\} + \frac{2\bar{\alpha}(k-1)}{\sin(2\phi)\sin(\theta)}\{[1 - \sin(\phi)\sin(\theta)]\cos^4(\phi)\sin^{2k}(\phi) + [\cos(\phi)\sin(\theta) - 1]\sin^4(\phi)\cos^{2k}(\phi)\}\right], \tag{22}$$

$$F_{\alpha,\alpha} = E_\alpha[H_{\alpha,\alpha}] + \sigma_\alpha^{-2} = 4\frac{\mathbf{s}^T \mathbf{s}}{\sigma_n^2} \left[\frac{\sin^{2k-2}(\theta)}{\sin^2(2\phi)}\{[\sin(\phi)\sin(\theta) - 1]^2 \cos^2(\phi)\sin^{2k}(\phi) + [\cos(\phi)\sin(\theta) - 1]^2 \sin^2(\phi)\cos^{2k}(\phi)\}\right.$$

$$\left. + \{\cos(\theta) - 1\}^2 \cos^{2k-2}(\theta)\right] + \frac{1}{\sigma_\alpha^2}. \tag{23}$$

The hybrid Cramér-Rao bounds for a triad of kth-order cardioids equal

$$\text{HCRB}(\theta) = \left[\{\mathbf{F}(\xi)\}^{-1}\right]_{1,1}; \tag{24}$$

$$\text{HCRB}(\phi) = \left[\{\mathbf{F}(\xi)\}^{-1}\right]_{2,2}; \tag{25}$$

$$\text{HCRB}(\alpha) = \left[\{\mathbf{F}(\xi)\}^{-1}\right]_{3,3}. \tag{26}$$

Of special practical interest is the first-order cardioid. This specific case will be investigated in great detail in Sec. IV.

IV. HYBRID CRAMÉR-RAO BOUND DERIVATION FOR FIRST-ORDER CARDIOIDS

Most practical cardioid sensors are of the first order, i.e., $k = 1$. In this case, Eqs. (18)–(23) may be simplified to give the following expressions for the elements of the HFIM:

$$F_{\theta,\theta} = \frac{\mathbf{s}^T\mathbf{s}}{\sigma_n^2}\left\{(1-\bar{\alpha})^2 + \sigma_\alpha^2\right\},$$

$$F_{\theta,\phi} = 0,$$

$$F_{\theta,\alpha} = \frac{\mathbf{s}^T\mathbf{s}}{\sigma_n^2}(1-\bar{\alpha})\left\{\cos(\theta)[\sin(\phi)+\cos(\phi)]-\sin(\theta)\right\},$$

$$F_{\phi,\phi} = \frac{\mathbf{s}^T\mathbf{s}}{\sigma_n^2}\left[(1-\bar{\alpha})^2 + \sigma_\alpha^2\right]\sin^2(\theta),$$

$$F_{\phi,\alpha} = \frac{\mathbf{s}^T\mathbf{s}}{\sigma_n^2}(1-\bar{\alpha})[\cos(\phi)-\sin(\phi)]\sin(\theta),$$

$$F_{\alpha,\alpha} = 2\frac{\mathbf{s}^T\mathbf{s}}{\sigma_n^2}\left\{2-\cos(\theta)-\sin(\theta)[\cos(\phi)+\sin(\phi)]\right\}+\frac{1}{\sigma_\alpha^2}.$$

From the above, Eqs. (24)–(26) become

$$\text{HCRB}(\theta) = \left[\{\mathbf{F}(\xi)\}^{-1}\right]_{1,1}$$
$$= \frac{\mathcal{A}}{\mathcal{A}+1}\frac{\dfrac{\mathcal{A}+1}{\mathcal{P}}+D_3(\theta,\phi)-2(\mathcal{A}+1)D_1(\theta,\phi)}{\mathcal{P}[D_2(\theta,\phi)-2\mathcal{A}D_1(\theta,\phi)]+\mathcal{A}+1}, \tag{27}$$

$$\text{HCRB}(\phi) = \left[\{\mathbf{F}(\xi)\}^{-1}\right]_{2,2}$$
$$= \frac{\mathcal{A}}{\mathcal{A}+1}\frac{\dfrac{\mathcal{A}+1}{\mathcal{P}}+D_4(\theta,\phi)-2(\mathcal{A}+1)D_1(\theta,\phi)}{\mathcal{P}[D_2(\theta,\phi)-2\mathcal{A}D_1(\theta,\phi)]+\mathcal{A}+1}$$
$$\times\frac{1}{D_5(\theta,\phi)}, \tag{28}$$

$$\frac{\text{HCRB}(\alpha)}{(1-\bar{\alpha})^2} = \frac{\left[\{\mathbf{F}(\xi)\}^{-1}\right]_{3,3}}{(1-\bar{\alpha})^2}$$
$$= \frac{\mathcal{A}(\mathcal{A}+1)}{\mathcal{P}[D_2(\theta,\phi)-2\mathcal{A}D_1(\theta,\phi)]+\mathcal{A}+1}, \tag{29}$$

where

$$\mathcal{A} := \left(\frac{\sigma_\alpha}{1-\bar{\alpha}}\right)^2,$$

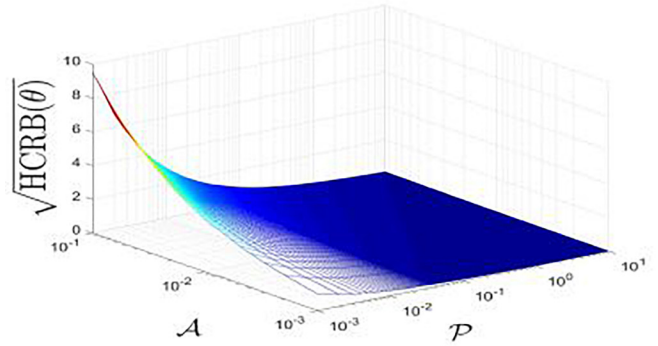$$\mathcal{P} := \sigma_\alpha^2\frac{\mathbf{s}^T\mathbf{s}}{\sigma_n^2},$$

$$D_1(\theta,\phi) := \cos(\theta)+[\sin(\phi)+\cos(\phi)]\sin(\theta)-2,$$

$$D_2(\theta,\phi) := 2\{1-\cos(\theta)\}\{1-\sin(\theta)$$
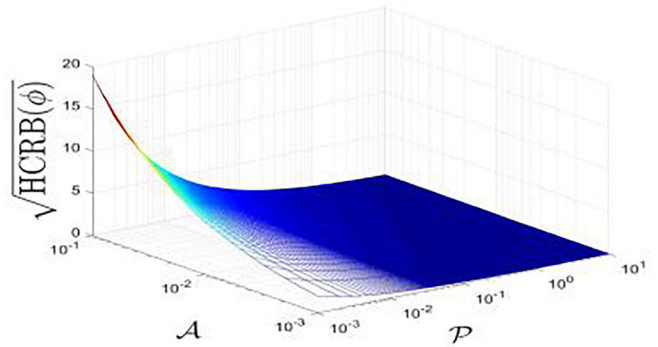$$\times[\sin(\phi)+\cos(\phi)]\}+\sin(2\phi)\sin^2(\theta),$$

$$D_3(\theta,\phi) := \sin(2\phi)-1,$$

$$D_4(\theta,\phi) := \sin(2\theta)[\sin(\phi)+\cos(\phi)]$$
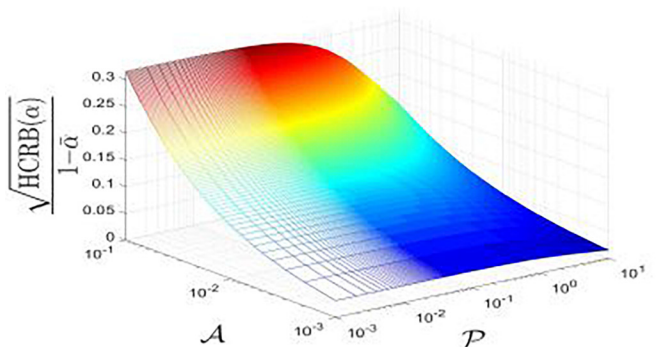$$-\cos^2(\theta)\sin(2\phi)-1,$$

$$D_5(\theta,\phi) := \sin^2(\theta).$$

(a) How $\sqrt{\text{HCRB}(\theta)}$ of (27) varies with $\mathcal{A}$ and versus $\mathcal{P}$.

(b) How $\sqrt{\text{HCRB}(\phi)}$ of (28) varies with $\mathcal{A}$ and versus $\mathcal{P}$.

(c) How $\sqrt{\text{HCRB}(\alpha)}$ of (29) varies with $\mathcal{A}$ and versus $\mathcal{P}$.

FIG. 3. (Color online) The first-order cardioid-triad's HCRBs at various values of $\mathcal{A} := (\sigma_\alpha/1-\bar{\alpha})^2$ and various values of $\mathcal{P} := \sigma_\alpha^2(\mathbf{s}^T\mathbf{s}/\sigma_n^2)$.

These hybrid Cramér-Rao bounds are expressed implicitly in terms of $\mathbf{s}^T\mathbf{s}$ inside $\mathcal{P}$; hence, these bounds apply to *any* real-valued waveform, whether wideband or narrowband, whether time-varying or time-invariant, whether stationary or non-stationary, whether zero-mean or otherwise—thereby offering high flexibility and thus wide applicability.

V. HYBRID CRAMÉR-RAO BOUND CHARACTERISTICS

For first-order cardioids, HCRB(θ), HCRB(ϕ), HCRB(α)/$(1-\bar{\alpha})^2$, each has exactly only four degrees of freedom—$\mathcal{A}$, $\mathcal{P}$, θ, and ϕ—even though the measurement data model has more degrees of freedom than four. A larger σ_α would increase both $\mathcal{A}$ and $\mathcal{P}$, but a larger $\bar{\alpha}$ would increase only $\mathcal{A}$ but not $\mathcal{P}$.

These three hybrid Cramér-Rao bounds are plotted in Fig. 3 versus $\mathcal{A}$ and versus $\mathcal{P}$ at $(\theta, \phi) = (30°, 45°)$.

These three hybrid Cramér-Rao bounds are also plotted in Figs. 3–6, at various $\mathcal{A}$ and $\mathcal{P}$. Each figure has a 3×3 "matrix" of sub-figures with $\mathcal{P}$ increasing rightward in this 3×3 matrix of sub-figures, and $\mathcal{A}$ increasing downward.
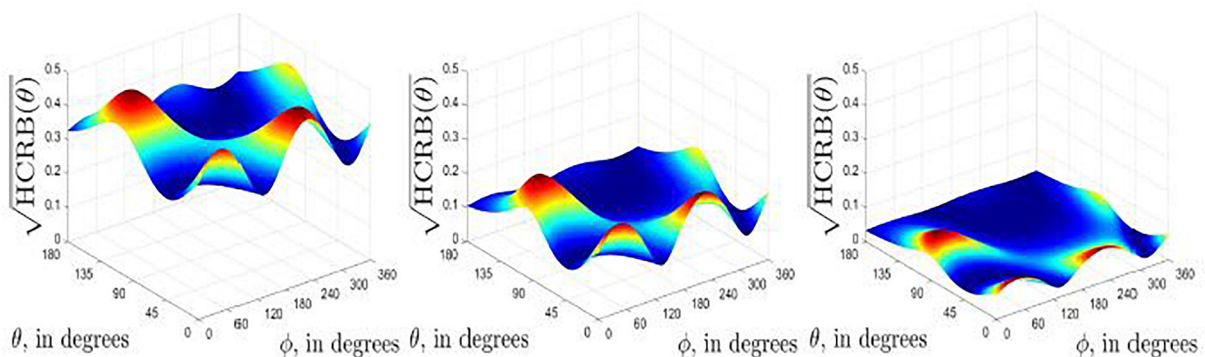
Qualitative observations on Figs. 4 and 5 are:

(a) Each HCRB in Fig. 3 increases monotonically with a decreasing $\mathcal{P}$ and an increasing $\mathcal{A}$.
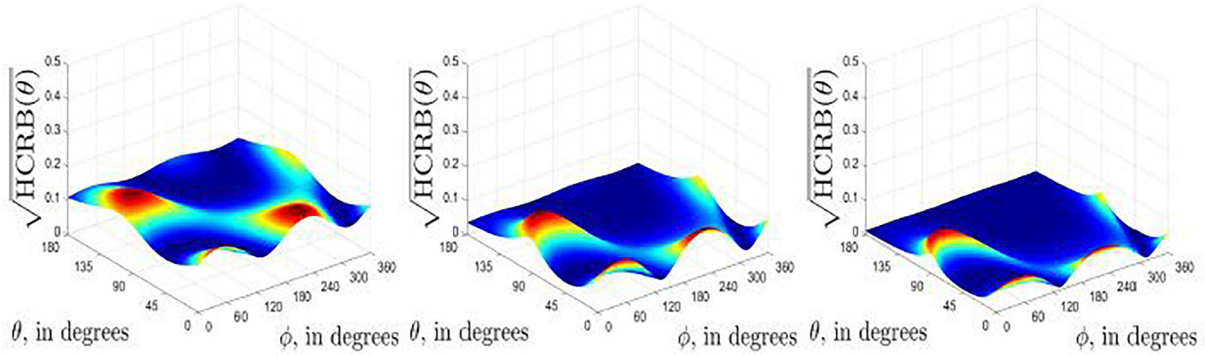
(a) $\mathcal{A} = 0.01$ and $\mathcal{P} = 1$.   (b) $\mathcal{A} = 0.01$ and $\mathcal{P} = 10$.   (c) $\mathcal{A} = 0.01$ and $\mathcal{P} = 100$.
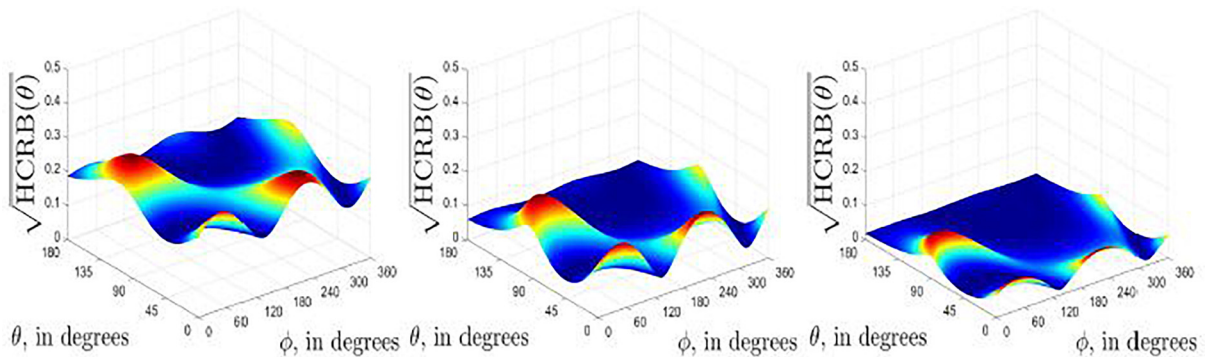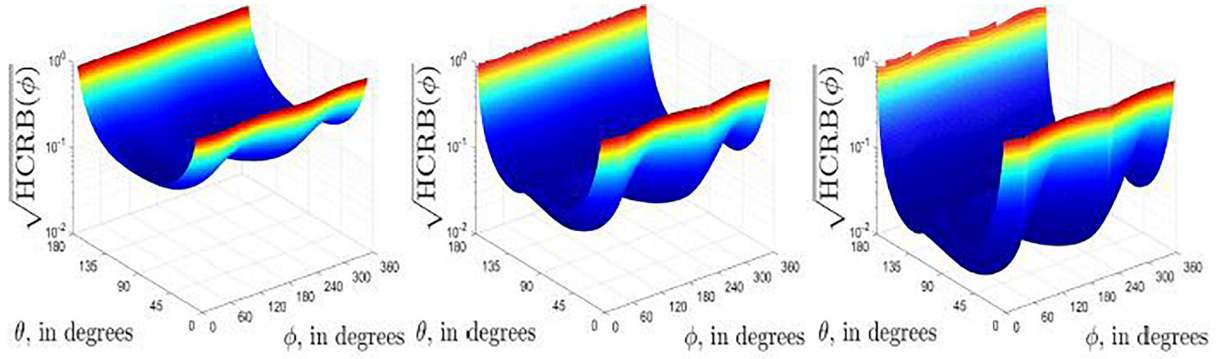
(d) $\mathcal{A} = 0.03$ and $\mathcal{P} = 1$.   (e) $\mathcal{A} = 0.03$ and $\mathcal{P} = 10$.   (f) $\mathcal{A} = 0.03$ and $\mathcal{P} = 100$.
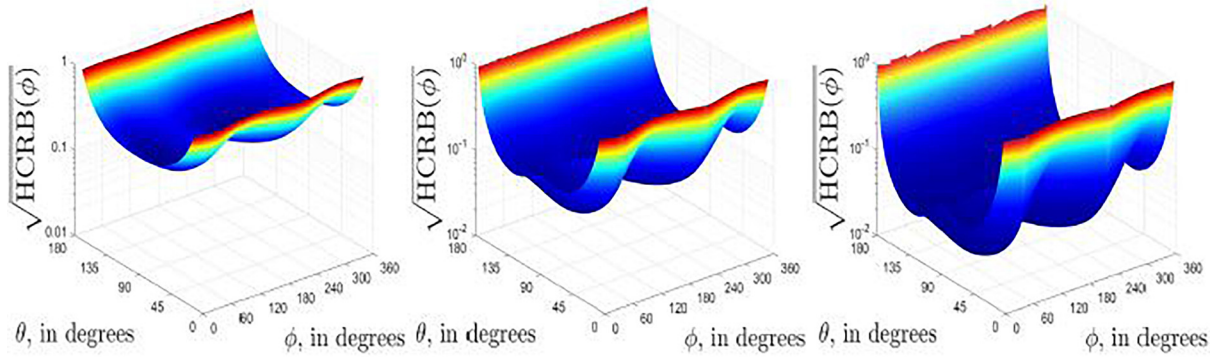
(g) $\mathcal{A} = 0.1$ and $\mathcal{P} = 1$.   (h) $\mathcal{A} = 0.1$ and $\mathcal{P} = 10$.   (i) $\mathcal{A} = 0.1$ and $\mathcal{P} = 100$.

FIG. 4. (Color online) The first-order cardioid-triad's HCRB(θ) at different values of $\mathcal{A} := (\sigma_\alpha/1 - \bar{\alpha})^2$ and $\mathcal{P} := \sigma_\alpha^2(\mathbf{s}^T\mathbf{s}/\sigma_n^2)$. Refer to Eq. (27).

J. Acoust. Soc. Am. **146** (2), August 2019

Kitavi *et al.*   1105

(a) $\mathcal{A} = 0.01$ and $\mathcal{P} = 1$. (b) $\mathcal{A} = 0.01$ and $\mathcal{P} = 10$. (c) $\mathcal{A} = 0.01$ and $\mathcal{P} = 100$.

(d) $\mathcal{A} = 0.03$ and $\mathcal{P} = 1$. (e) $\mathcal{A} = 0.03$ and $\mathcal{P} = 10$. (f) $\mathcal{A} = 0.03$ and $\mathcal{P} = 100$.

(g) $\mathcal{A} = 0.1$ and $\mathcal{P} = 1$. (h) $\mathcal{A} = 0.1$ and $\mathcal{P} = 10$. (i) $\mathcal{A} = 0.1$ and $\mathcal{P} = 100$.
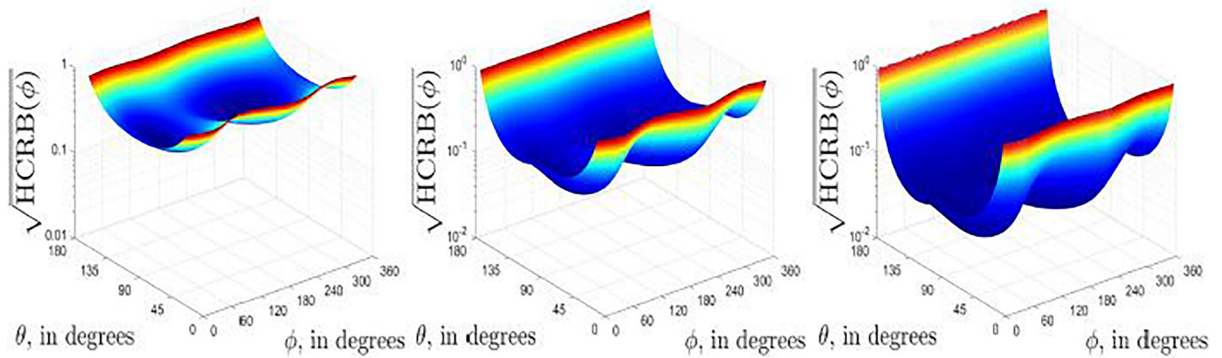
FIG. 5. (Color online) The first-order cardioid-triad's HCRB(ϕ) at different values of $\mathcal{A} := (\sigma_\alpha/1 - \bar{\alpha})^2$ and $\mathcal{P} := \sigma_\alpha^2(\mathbf{s}^T\mathbf{s}/\sigma_n^2)$. Refer to Eq. (28).

(b) As $\mathcal{A}$ increases or as $\mathcal{P}$ decreases, both HCRB(θ) and HCRB(ϕ) and HCRB(α)/$(1 - \bar{\alpha})^2$ will all increase for any constant (θ,ϕ). This is largely due to the increasing vertical displacement.

(c) HCRB(θ) and HCRB(ϕ) vary much less with (θ,ϕ) than with $\mathcal{A}$ or $\mathcal{P}$.

Figure 5 has a shape dominated by the $\sin^2(\theta)$ factor in the denominator. This is physically due to little acoustical energy projected onto the x-y plane on which ϕ is defined.

(d) (e) HCRB(ϕ) $\rightarrow \infty$ as $\theta \rightarrow 0, \pi$. This is because Eq. (28) has a factor of $\sin^2(\theta)$ in its denominator.

For $\sigma_\alpha^2 = 0$, Eqs. (27) and (28) reduce to

$$\text{HCRB}(\theta) = \frac{\sigma_n^2}{\mathbf{s}^T\mathbf{s}} \frac{1}{(1 - \bar{\alpha})^2}, \tag{30}$$

$$\text{HCRB}(\phi) = \frac{\sigma_n^2}{\mathbf{s}^T\mathbf{s}} \frac{\csc^2(\theta)}{(1 - \bar{\alpha})^2}. \tag{31}$$

Substituting $\bar{\alpha}$ for α, one obtains Eqs. (30) and (31), which are the Cramér-Rao bounds for a deterministic $\alpha = \bar{\alpha}$. The expressions suggest that a smaller cardioidicity index $\alpha = \bar{\alpha}$ could increase (i.e., could worsen) an unbiased
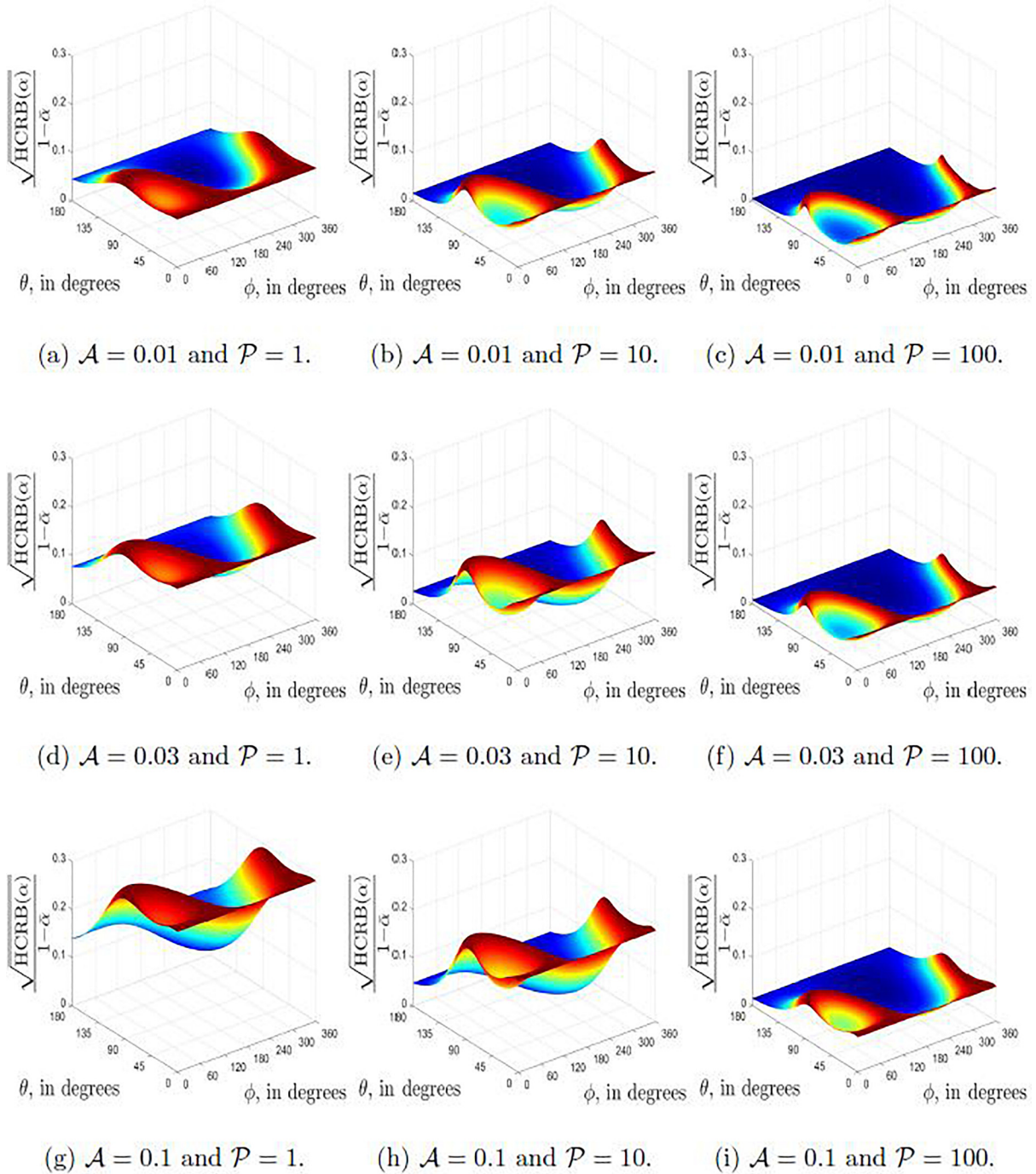
FIG. 6. (Color online) The first-order cardioid-triad's HCRB(α) at different values of $\mathcal{A} := (\sigma_\alpha/1 - \bar{\alpha})^2$ and $\mathcal{P} := \sigma_\alpha^2(\mathbf{s}^T\mathbf{s}/\sigma_n^2)$. Refer to Eq. (29).

estimator's error variance. The worst cardioidicity index is $\alpha = \bar{\alpha} = 0$, corresponding to the customary tri-axial velocity-sensor mentioned in Sec. I.

VI. MAXIMUM *A POSTERIORI* (MAP) ESTIMATION OF THE AZIMUTH-ELEVATION DIRECTION-OF-ARRIVAL

The probability density function of the observation $\mathbf{z}$, given $\boldsymbol{\xi} := [\theta, \phi, \alpha]$, equals

$$p(\mathbf{z}|\boldsymbol{\xi}) = |2\pi\Gamma|^{-1/2} \exp\left(-\frac{1}{2}[\mathbf{z}-\boldsymbol{\mu}]^T\Gamma^{-1}[\mathbf{z}-\boldsymbol{\mu}]\right), \quad (32)$$

whereas the probability density function of α is

$$p(\alpha) = \frac{1}{\sqrt{2\pi}\sigma_\alpha} \exp\left(-\frac{(\alpha-\bar{\alpha})^2}{2\sigma_\alpha^2}\right).$$

Hence, for $\boldsymbol{\xi}$ given the observation $\mathbf{z}$, the posterior probability density function equals

$$p(\boldsymbol{\xi}|\mathbf{z}) \propto p(\boldsymbol{\xi}, \mathbf{z}) = p(\mathbf{z}|\boldsymbol{\xi})\,p(\alpha)$$

$$= \frac{1}{2\pi\sigma_\alpha\sqrt{|2\pi\Gamma|}} \exp\left(-\frac{1}{2\sigma_n^2}[\mathbf{z}-\boldsymbol{\mu}]^T[\mathbf{z}-\boldsymbol{\mu}]\right.$$

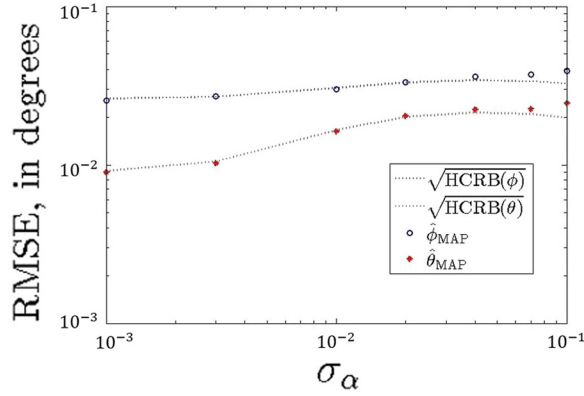$$\left. -\frac{(\alpha-\bar{\alpha})^2}{2\sigma_\alpha^2}\right).$$

FIG. 7. (Color online) The MAP estimates of Eq. (33) approach HCRB(θ) and HCRB(ϕ), which are derived in Eqs. (27) and (28). Here, the cardioid order equals $k = 1$.

The MAP estimate ($\hat{\boldsymbol{\xi}}_{\mathrm{MAP}}$) of $\boldsymbol{\xi}$ given $\mathbf{z}$ by definition equals

$$
\begin{aligned}
\left(\hat{\theta}, \hat{\phi}, \hat{\alpha}\right) &:= \arg\max_{(\theta,\phi,\alpha)} p(\boldsymbol{\xi}|\mathbf{z}) \\
&= \arg\max_{(\theta,\phi,\alpha)} p(\mathbf{z}|\boldsymbol{\xi}) \, p(\alpha) \\
&= \arg\max_{(\theta,\phi,\alpha)} \left\{ \frac{[\mathbf{z} - \boldsymbol{\mu}]^T [\mathbf{z} - \boldsymbol{\mu}]}{\sigma_n^2} + \frac{(\alpha - \bar{\alpha})^2}{\sigma_\alpha^2} \right\}.
\end{aligned}
$$

(33)

The above minimization in Eq. (33) may be solved iteratively via MATLAB's built-in function of *fminsearch*.

Figures 7 and 8, respectively, for order $k = 1$ and $k = 2$, show that this MAP estimator and the earlier derived HCRBs indeed approach each other. Here in Figs. 7 and 8, $\bar{\alpha} = \frac{1}{2}$, $(\theta, \phi) = (20°, 60°)$, $\sigma_n = 0.1$, $s(m) = \cos(0.6\pi m)$, and there exist $P = 1000$ Monte Carlo independent trials for each icon. The root-mean-square error (RMSE) is defined as $\sqrt{(1/P) \sum_{p=1}^{P} (\hat{\theta}_p - \theta)^2}$ for the polar arrival angle, and $\sqrt{(1/P) \sum_{p=1}^{P} (\hat{\phi}_p - \phi)^2}$ for the azimuth arrival angle, with $(\hat{\theta}_p, \hat{\phi}_p)$ representing the pth Monte Carlo trial's estimate.
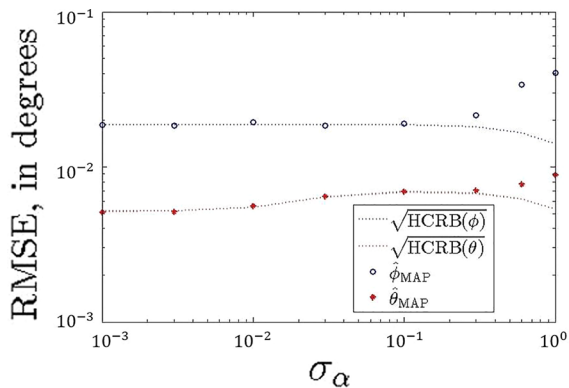

FIG. 8. (Color online) The MAP estimates of Eq. (33) approach HCRB(θ) and HCRB(ϕ), which are derived in Eqs. (24) and (25). Here, the cardioid order equals $k = 2$.
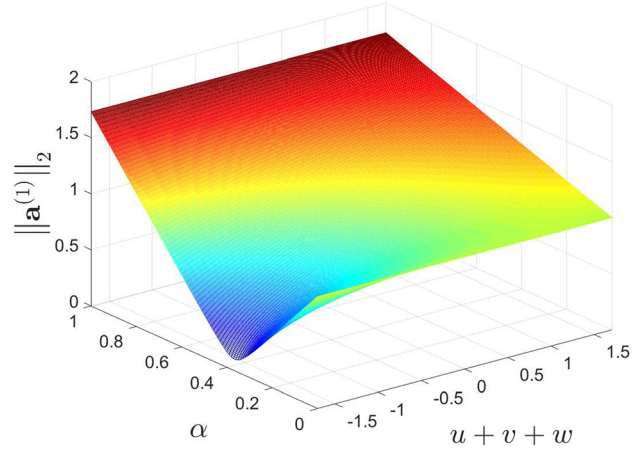

FIG. 9. (Color online) How $\|\mathbf{a}^{(1)}\|_2$ varies non-monotonically with α and $\{u + v + w\}$.

Figures 7 and 8 also reveal that the HCRBs could decrease with *in*creasing randomness in α (i.e., as σ_α increases). This might surprise some readers. This phenomenon arises from the cardioid triad's array manifold having a Frobenius norm that varies with α (besides varying also with k, θ, ϕ). For example, at order $k = 1$,

$$
\|\mathbf{a}^{(1)}\|_2 = \sqrt{3\alpha^2 + (1 - \alpha)^2 + 2\alpha(1 - \alpha)[u + v + w]}.
$$

(34)

This $\|\mathbf{a}^{(1)}\|_2$ is plotted in Fig. 9 versus $\alpha \in [0, 1]$ and versus $u + v + w \in [-1.7071, 1.7071]$. There, $\|\mathbf{a}^{(1)}\|_2$ is revealed to vary *not* monotonically with changing α. Rather, as α increases from zero toward unity, $\|\mathbf{a}^{(1)}\|_2$ would increase, then would decrease, and finally would increase again. This pattern is more pronounced for smaller $u + v + w$.

VII. CONCLUSION

This paper advances the idea of placing three cardioid microphones/hydrophones (of any cardioidic order k) in orthogonal orientation but spatial collocation for frequency-independent direction finding—to the best of our knowledge. This paper has analytically derived the corresponding hybrid Cramér-Rao bound for direction finding. This derivation allows for stochastic uncertainty in the cardioidic index α. Quite surprisingly, the hybrid Cramér-Rao bounds are found *not* to decrease with increasing uncertainty in α, and this is found to be explainable by the array manifold's Frobenius norm being non-monotonically dependent on α. At first order $k = 1$, (a) the hybrid Cramér-Rao bounds turn out to have only four degrees of freedom: the polar-azimuth direction-of-arrival (θ, ϕ), $\mathcal{A} := (\sigma_\alpha/(1 - \bar{\alpha}))^2$ and $\mathcal{P} := \sigma_\alpha^2(\mathbf{s}^T\mathbf{s}/\sigma_n^2)$, and (b) a larger cardioidicity index $\alpha = \bar{\alpha}$ could improve an unbiased estimator's error variance.

1108   J. Acoust. Soc. Am. **146** (2), August 2019

Kitavi *et al.*

[1]J. Eargle, *The Microphone Book*, second ed. (Focal Press, Burlington, MA, 2005).

[2]H. F. Olson, *Acoustical Engineering* (Van Nostrand Co., Princeton, NJ, 1957).

[3]W. Woszczyk, "A microphone technique applying to the principle of second-order gradient unidirectionality," J. Audio Eng. Soc. **32**(7/8), 507–530 (1984).

[4]B. R. Beavers and R. Brown, "Third-order gradient microphone for speech reception," J. Audio Eng. Soc. **18**(6), 636–640 (1970).

[5]A. Y. Olenko and K. T. Wong, "Noise statistics across the three axes of a tri-axial velocity sensor constructed of pressure sensors," IEEE Trans. Aerosp. Electron. Syst. **51**(2), 843–852 (2015).

[6]Y. Huang and J. Benesty (editors), *Audio Signal Processing for Next-Generation Multimedia Communication Systems* (Kluwer Academic Publishers, Boston, MA, 2004).

[7]C. H. Sherman and J. L. Butler, *Transducers and Arrays for Underwater Sound* (Springer Science and Business Media, New York, 2007).

[8]I. J. Tashev, *Sound Capture and Processing, Practical Approaches* (Wiley, Chichester, U.K., 2013).

[9]M. R. Bai, J.-G. Ih, and J. Benesty, *Acoustic Array Systems Theory, Implementation, and Application* (Wiley, Singapore, 2013).

[10]R. P. Glover, "A Review of cardioid type unidirectional microphones," J. Acoust. Soc. Am. **11**(3), 296–302 (1940).

[11]H. F. Olson, "The quest for directional microphones at RCA," J. Audio Eng. Soc. **28**(11), 776–786 (1980).

[12]K. T. Wong, C. J. Nnonyelu, and Y. I. Wu, "A triad of cardioid sensors in orthogonal orientation and spatial collocation—Its spatial-matched-filter-type beam-pattern," IEEE Trans. Signal. Proc. **66**(4), 865–906 (2018).

[13]A. Nehorai and E. Paldi, "Acoustic vector-sensor array processing," IEEE Trans. Signal. Proc. **42**(10), 2481–2491 (1994).

[14]K. T. Wong and M. D. Zoltowski, "Closed-form underwater acoustic direction-finding with arbitrarily spaced vector-hydrophones at unknown locations," IEEE J. Ocean. Eng. **22**(3), 566–575 (1997).

[15]P. K. Tam and K. T. Wong, "Cramér-Rao bounds for direction finding by an acoustic vector-sensor under non-ideal gain-phase responses, non-collocation, or non-orthogonal orientation," IEEE Sens. J. **9**(8), 969–982 (2009).

[16]K. T. Wong, "Acoustic vector-sensor 'blind' beamforming and geolocation for FFH-sources," IEEE Trans. Aerosp. Electron. Syst. **46**(1), 444–449 (2010).

[17]Y. I. Wu and K. T. Wong, "Acoustic near-field source localization by two passive anchor nodes," IEEE Trans. Aerosp. Electron. Syst. **48**(1), 159–169 (2012).

[18]Y. I. Wu, K. T. Wong, S.-k. Lau, X. Yuan, and S.-k. Tang, "A directionally tunable but frequency-invariant beamformer on an acoustic velocity-sensor triad to enhance speech perception," J. Acoust. Soc. Am. **131**(5), 3891–3902 (2012).

[19]C. J. Nnonyelu, Y. I. Wu, and K. T. Wong, "Cardioid microphones/hydrophones in a collocated and orthogonal triad a steerable beamformer with no beam-pointing error," J. Acoust. Soc. Am. **145**(1), 575–588 (2019).

[20]F. Massa, "Directional energy receiving systems for use in the automatic indication of the direction of arrival of the received signal," J. Acoust. Soc. Am. **68**(6), 1912–1913 (1980).

[21]K. Freiberger and A. Sontachi, "Similarity-based sound source localization with a coincident microphone array," in *International Conference on Digital Audio Effects*, Paris, France (September 2011), pp. 185–190.

[22]N. Vryzas, C. A. Dimoulas, and G. V. Papanikolaou, "Embedding sound localization and spatial audio interaction through coincident microphones arrays," in *Audio Mostly Conference on Interaction with Sound*, Thessaloniki, Greece (October 7–9, 2015), article 36.

[23]H. Cox, "Super-directivity revisited," in *IEEE Instrumentation and Measurement Technology Conference* (2004), pp. 877–880.

[24]H. Cox and H. Lai, "Performance of line arrays of vector and higher order sensors," in *Forty-First Asilomar Conference on Signals, Systems and Computers* (2007), pp. 1231–1236.

[25]J. A. Clark, "High-order angular response beamformer for vector sensors," J. Sound Vib. **318**(3), 417–422 (2008).

[26]B. A. Cray and A. H. Nuttal, "Directivity factors for linear arrays of velocity sensors," J. Acoust. Soc. Am. **110**(1), 324–331 (2001).

[27]H. E. de Bree, T. Basten, and D. Yntema, "A single broad banded 3D beamforming sound probe," in *German Annual Conference on Acoustics* (2008).

[28]R. M. M. Derkz and K. Janse, "Theoretical analysis of a first-order azimuth-steerable superdirective microphone array," IEEE Trans. Audio Speech Lang. Proc. **17**(1), 150–162 (2009).

[29]G. L. D'Spain, J. C. Luby, G. R. Wilson, and R. A. Gramann, "Vector sensors and vector sensor line arrays: Comments on optimal array gain and detection," J. Acoust. Soc. Am. **120**(1), 171–185 (2006).

[30]B. Gur, "Particle velocity gradient based acoustic mode beamforming for short linear vector sensor arrays," J. Acoust. Soc. Am. **135**(6), 3463–3473 (2014).

[31]K. B. Smith and A. V. V. Leijen, "Steering vector sensor array elements with linear cardioids and nonlinear hippioids," J. Acoust. Soc. Am. **122**(1), 370–377 (2007).

[32]O. B. Wilson, S. N. Wolf, and F. Ingenito, "Measurements of acoustic ambient noise in shallow water due to breaking surf," J. Acoust. Soc. Am. **78**(1), 190–195 (1985).

[33]H. L. Van Trees, *Detection, Estimation and Modulation Theory, Part IV: Optimum Array Processing* (Wiley, New York, 2002).